Secondary calibrators for continuum measurements in the 1.3mm window at the IRAM 30m telescope

U. Lisenfeld, C. Thum, R. Neri, A. Sievers

November 17, 2000

1 Introduction

In order to calibrate bolometer observations one needs to compare them to the measurement of a source with a well known flux. The best calibrators are some of the planets (Mars, Uranus, Neptune – see Kramer [1997] for a discussion of the use of the planets for calibration). Unfortunately, the planets sometimes are only visible at inconvenient times, e.g. during the day when good data quality necessary for calibration cannot be achieved. Because of this, it is desirable to have a group of "secondary" calibrators, i.e. objects, that are calibrated with respect to the planets, and that can be observed at any LST.

For this aim we have started to observe a group of potential secondary calibrators. The observations were carried out in spring 1999 and spring 2000 with the MPIfR 37-channel bolometer (MAMBO) mounted in the nasmyth focus of the IRAM 30m telescope. The measurements included mapping of the objects in order to determine their shape and extent and onoff measurements yielding their flux density per beam. The main result consists in a table of flux densities per beam of the secondary calibrators that can be used for the calibration of other astronomical sources.

2 Source selection

An ideal calibrator should be bright and compact (small with respect to the beam) and its flux should not vary in time. Furthermore, the objects in our sample should be well distributed in LST so that it is possible at any time to measure a calibrator.

In Table 1 we list the selected candidates and their positions. The objects were taken from Altenhoff, Thum & Wendker (1994), Sandell (1996), Dutrey et al. (1996) and Sánchez Contreras et al. (1998). They belong to the following groups of objects:

1. Protostellar objects, pre-main sequence and young stars: These objects are usually very compact, but only few are strong enough to be used as calibrators.

2. Ultracompact HII regions: They are usually strong millimetre emitters, but often associated with extended emission.

3. Evolved stars (AGB stars, planetaries, protoplanetaries): They are also strong millimetre emitters, but frequently extended and their flux may be variable in time.

Table 1: Source coordinates

Name	R.A. (2000)	Dec (2000)
Protostellar objects, pre-main sequence and young stars		
GL 490	03:27:38.8342	58:47:00.719
L1551 IRS5	04:31:34.1541	18:08:05.163
HL Tau	04:31:38.4437	18:13:57.978
LkHα 234	21:43:06.7208	66:06:54.618
Ultracompact HII regions		
W3(OH)	02:27:03.8653	61:52:24.829
G34.3	18:53:18.5105	01:14:58.225
G45.1	19:13:22.0201	10:50:53.392
K3-50A	20:01:45.6374	33:32:43.548
NGC 7538	23:13:45.3318	61:28:10.572
Evolved stars: AGB stars, planetaries, protoplanetaries		
CRL 618	04:42:53.3448	36:06:52.750
ALF Ori	05:55:10.2737	07:24:25.393
CW Leo	09:47:57.2726	13:16:43.785
MWC 349	20:32:45.5141	40:39:36.547
CRL 2688	21:02:18.7458	36:41:37.780
NGC 7027	21:07:01.5322	42:14:10.287
CepA	22:56:17.8735	62:01:49.793
Asteroids		
Ceres		

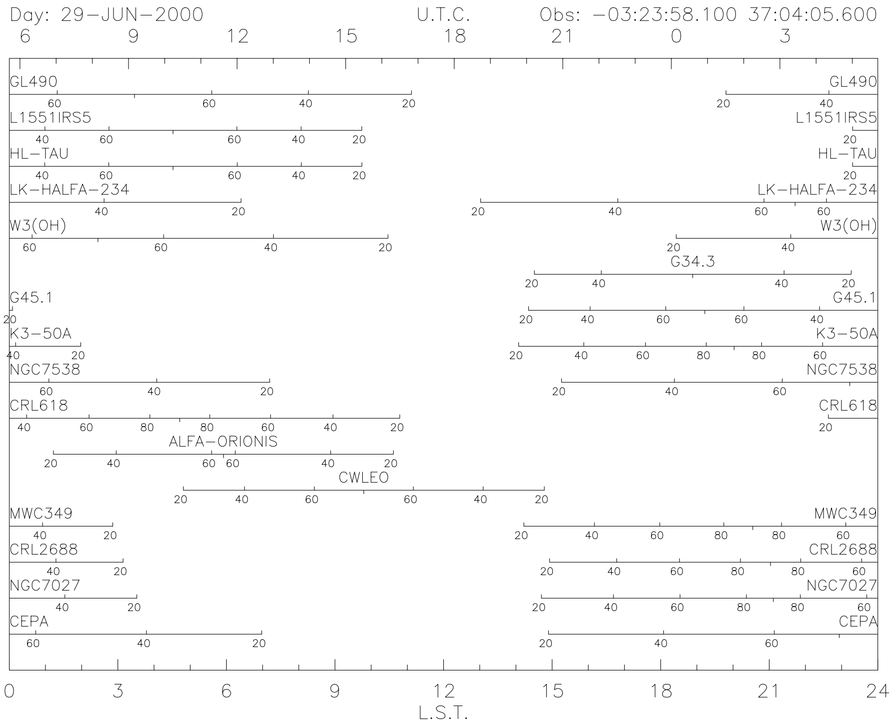

Figure 1: The distribution of the objects in Declination and Right Ascension

4. Asteroids: The strongest asteroids might be, in a similar way as the planets, very useful calibrators. They have been successfully used for calibration of ISOPHOT data (Müller & Lagerros 1998). We have observed Ceres, the brightest planetoid, in order to test whether this class of objects is suited to be used as a secondary calibrator. Ceres has shown to be clearly strong enough, but further work – beyond the scope of the present project – would be necessary in order to predict the variations of its flux before it can be used as a calibrator.

In Fig.1 the visibility of the objects from Table 1 is shown. In general, it is very hard to find an object which is strong and point-like at the same time. We have applied the following selection criterias:

- Compactness: We have excluded objects that show very extended emission. Some of the objects in our list do still show weak extended emission. We found them acceptable as secondary calibrators if the extended emission at distance of the wobbler throw (about $50''$) was below 5% of the peak emission.

- Strength: The flux density of the secondary calibrator has to be at least a few 100 mJy, the limit necessary to allow a pointing measurement on the source before the onoff measurement. This requirement ensures that the pointing error is minimized.

- Flux constancy: The flux densities of the objects in our list do not vary in time, except for CW Leo (= IRC+10216) which shows a long-term variability with a period of about 635 days (JCMT homepage) and a flux variation of about 40% (Sandell 1994). We kept CW Leo nevertheless, since its periodicity is known and it is situated at a position on the sky where there are no other secondary calibrators.

3 Observations and data reduction

The secondary calibrators were observed with the MPIfR 37-channel bolometer (MAMBO) in spring 1999 and 2000. Some of the maps were done in December 1998 with the 19-channel bolometer.

The observing procedure was in all cases the same: A pointing measurement was carried out on the object and afterwards one or two onoffs, each normally with 16 subscan of 10 s. The wobbler throw ranged between 46" and 50" and the period was 0.5 s.

Furthermore maps were obtained for all objects in order to determine their sizes and shapes. From the maps the source sizes were derived by performing a Gaussian fit yielding the full width half maximum (FWHM) of the source convolved with the beam. The source size can then be calculated, assuming that both the beam and the source are gaussian, by

$$\Theta_s^2 = \Theta^2 - \Theta_b^2. \tag{1}$$

where Θ_s is the FWHM of the source, Θ the FWHM of the source convolved with the beam and Θ_b the HPBW. $\Theta_b = 10.8''$ was adopted for all maps.

The data were reduced in the standard way using the software package NIC (Broguière, Neri & Sievers 1998). The data reduction includes correction for the gain-elevation efficiency (adopting the gain-elevation curve given in the 30m manual [Wild 1999]) and for the sky opacity, subtraction of linear baselines and skynoise.

4 Calibration of the bolometer observation

4.1 Effective frequency

The bolometer bandpass is very broad. In order to calibrate the data, i.e. compare the counts measured with the bolometer to the flux of a planet at a certain frequency, we need to define the effective frequency of the observations, $\nu_{\rm eff}$. We do this in the following way. The total observed flux of a source is:

$$S_{tot} = \int_{\nu_l}^{\nu_h} S(\nu)A(\nu)T(\nu)d\nu. \tag{2}$$

$T(\nu)$ is the bandpass of the instrument with ν_l and ν_h being the lower and upper frequency limits, $A(\nu)$ is the atmospheric transmission and $S(\nu)$ the source spectrum which we approximate in the following by a power-law, $S(\nu) = S_0\nu^\alpha$, with exponent α. We neglect the frequency dependence of the aperture efficiency, η_a, and of the gain elevation correction because they are small (η_a changes less than 20 % and the gain-elevation correction less than 10% over the 80 GHz bandpass of MAMBO).

The average flux density observed in the bandpass is therefore:

$$< S >= \frac{S_{tot}}{\int_{\nu_l}^{\nu_h} A(\nu)T(\nu)d\nu} = \frac{S_0 \int_{\nu_l}^{\nu_h} \nu^\alpha S(\nu)T(\nu)d\nu}{\int_{\nu_l}^{\nu_h} A(\nu)T(\nu)d\nu}. \tag{3}$$

We define the effective frequency as the frequency at which the monochromatic flux density would be equal to the average flux density observed in the entire bolometer bandpass:

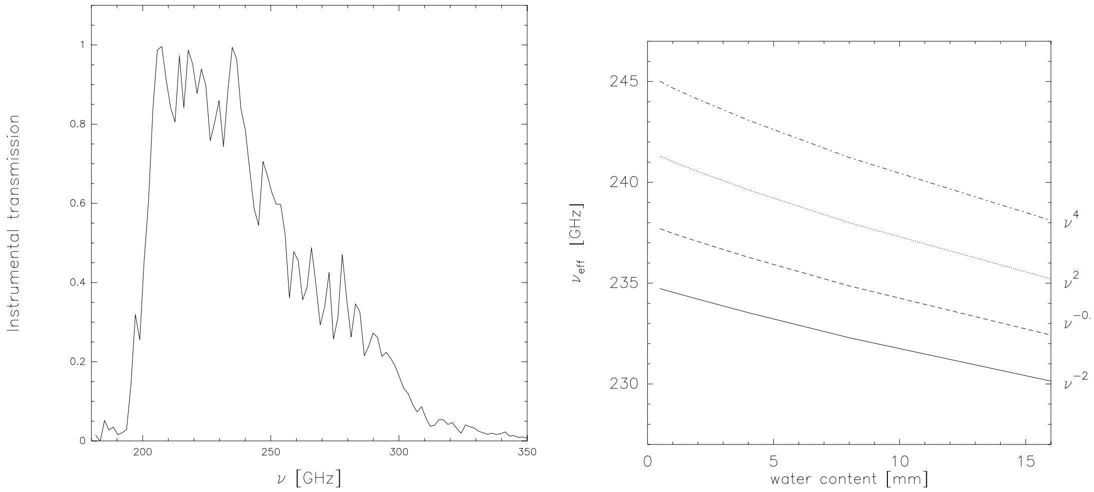

Figure 2: (a) The instrumental bandpass of MAMBO. (b) The effective frequency for MAMBO for different source spectral indices α as a function of water content in the atmosphere.

$$S_0 \nu_{eff}^{\alpha} =< S > . \tag{4}$$

Together with eq.(3) this yields

$$\nu_{\rm eff}^{\alpha} = \frac{\int_{\nu_l}^{\nu_h} \nu^{\alpha} A(\nu) T(\nu) {\rm d}\nu}{\int_{\nu_l}^{\nu_h} A(\nu) T(\nu) {\rm d}\nu}. \tag{5}$$

In Fig. 2a we show the adopted instrumental bandpass of MAMBO and in Fig. 2b the resulting $\nu_{\rm eff}$ for some typical source spectral indices. For the atmospheric transmission we have used the atmospheric model by Cernicharo (1985) (curves are in 30m manual).

We see that $\nu_{\rm eff}$ does depend on the water content in the atmosphere and the source spectral index, but the dependence is moderate. For a planet ($S(\nu) \propto \nu^2$) observed under reasonable conditions (water content $<$ 5 mm) $\nu_{\rm eff}$ is about 240 GHz. We will adopt this value for the calibration of our data.

The extreme values (for reasonable weather conditions) of $\nu_{\rm eff}$ are 245 GHz and 232 GHz (for $\alpha = 4$ at 0mm water and $\alpha = -2$ at 10mm water) instead of 240 GHz used for the calibration here. If we observe sources with such spectral indices under these weather conditions we make a calibration error of $(245/240)^2 = 4\%$ and $(240/232)^2 = 7\%$ because we have assumed the wrong planet flux for the calibration. Thus, we conclude that the error due to the unknown $\nu_{\rm eff}$ is below 10 %.

4.2 Adopted conversion factor

Ideally the calibration is done by observing a planet (Mars or Uranus) with the same observational parameters as the secondary calibrator and close in time in order to probe the same weather conditions. From the expected flux density per beam of the planet and the observed instrumental counts one can derive the conversion factor (counts/Jy) used to scale the counts measured on the secondary calibrator.

The expected fluxes densities per beam of the planets were derived using the software package ASTRO assuming a beamwidth of 10.8" and an effective frequency of 240 GHz.

For practical reasons the combined measurement of planets and secondary calibrators has mostly not been possible because, e.g. the planets and the secondary calibrators were not visible at the same time.

We have therefore chosen to calibrate the secondary data with the average conversion factor derived from good planet onoff observations during the whole season. The average conversion factor for spring 1999 is 5250 $\pm$ 440 counts/Jy beam^{-1} and for spring 2000 14200 $\pm$ 830 counts/Jy beam^{-1}. The standard deviation of the conversion factor is less than 10% showing that it is reasonable to adopt the average value. Furthermore, no temporal trend in the conversion factor is visible, the values simply scatter around the average value which might be an indication that the weather has the most important influence.

As a test, we have also derived the flux densities of the secondary calibrators with the individual calibration factors if such a measurement was available in the period of two days or less before or after the measurement of the secondary calibrator. The result is, within the error, identical to the results shown in the next section.

5 Results

5.1 Onoff measurements

In Table 2 we list the flux densities per beam obtained with the bolometers in spring 1999 and 2000 as well as the ratio between them. The error has been calculated as the standard deviation of the different measurements weighted with their statistical errors. The number in brackets indicates the number of individual observations.

The agreement between the measurements of the two years is generally very good. The average ratio between the data of spring 2000 and those of spring 1999 is 1.06 $\pm$ 0.09. There is no indication of a significant error in the conversion factor of one of the years which could be noticeable in a systematically higher or lower value of the corresponding data.

For L1551 IRS5 the difference between the 1999 and 2000 data is unacceptably large (30%). The reason for this difference is unclear, further measurements are necessary. Apart from this object only for NGC 7538, LkHα 234 and GL 490 the differences between the two years exceed 10%.

Surprisingly, we did not measure a difference between the flux densities of CW-Leo in the two years, although the emission of this object is variable. The period of its variation is 635 days (JCMT homepage) and its emission had a minimum on the 14th of July 1998. Thus, the next maximum should have occurred on the 24th of May 1999 and the next minimum on the 10th of April 2000 – both dates lying close to the spring observing period. The difference in flux between the minimum and maximum is supposed to be about 40% (Sandell 1994) so we would have expected to measure a different flux for the two years.

5.2 Maps

In Fig. 3 the maps of the sources are shown. Most of the sources are not point-like but are surrounded by extended emission. An important criterion for the selection of an object as a secondary calibrator is that these envelopes are weak in comparison with the central emission and that they are more or less symmetrical. This condition ensures that the result of an onoff

Table 2: Flux densities [Jy/beam] obtained with the bolometers

Name	spring 1999	spring 2000	2000/1999	average
GL 490	1.65 ± 0.04 (2)	1.85 ± 0.17 (4)	1.12	1.81 ± 0.18 (6)
L1551 IRS5	1.19± 0.02 (4)	1.55 ± 0.07 (7)	1.29	1.46 ± 0.17 (11)
HL Tau	0.81 ± 0.06 (3)	0.76 ± 0.05 (6)	1.07	0.80 ± 0.05 (9)
LkHα 234	0.86 ± 0.03 (9)	1.02 ± 0.06 (6)	1.19	0.96 ± 0.10 (15)
W3(OH)	6.74 ± 0.39 (7)	7.19 ± 0.41 (6)	1.07	6.98 ± 0.44 (13)
G34.3	20.10 ± 0.77 (4)	20.96 ± 0.43 (5)	1.04	20.43 ± 0.76 (9)
G45.1	2.55 ± 0.10 (4)	2.57 ± 0.27 (5)	1.00	2.56 ± 0.19 (9)
K3-50A	6.41 ± 0.19 (8)	6.34 ± 0.22 (7)	0.99	6.41 ± 0.19 (15)
NGC 7538	5.36 ± 0.31 (7)	6.16 ± 0.11 (6)	1.15	5.69 ± 0.48 (13)
CRL 618	2.66 ± 0.10 (4)	2.75 ± 0.20 (3)	1.04	2.67 ± 0.11 (7)
ALF Ori	0.30± 0.01 (4)	0.28 ± 0.01 (5)	1.08	0.29 ± 0.02 (9)
CW Leo	1.33 ± 0.05 (9)	1.31 ± 0.05 (10)	0.98	1.31 ± 0.05 (19)
MWC 349	1.71± 0.14 (4)	1.55 ± 0.07 (7)	0.90	1.62 ± 0.13 (11)
CRL 2688	1.87 ± 0.04 (5)	1.98 ±0.06 (3)	1.06	1.90 ± 0.07 (8)
NGC 7027	2.73± 0.04 (5)	2.86± 0.13 (7)	1.05	2.77 ± 0.10 (13)
CepA	3.67 ± 0.20 (4)	3.62 ± 0.12 (5)	0.98	3.65 ± 0.18 (9)
Ceres	1.23 ± 0.21 (4)	3.32 ± 0.13 (12)	n.a.	n.a.

Table 3: Deconvolved source sizes (major and minor axis) in arcsec

Name	1.2mm (IRAM)	800 μm (JCMT)
GL 490	$16.4 \times 11.3^{(1)}$	$< 5.00 \times 8.7$
L1551-IRS5	14.8×11.1	5.2×10.0
HL Tau	6.5×3.3	–
LkHα 234	21.2×14.3	–
W3(OH)	17.3×9.5	14.2×10.2
G34.3	$11.1 \times 9.2^{(2)}$	6.2×7.8
G45.1	$12.6 \times 9.4^{(2)}$	9.4×10.0
K3-50A	11.4×9.2	10.6×5.5
NGC 7538	15.8×13.0	20.4×17.6
CRL 618	5.7×4.5	< 5
ALF Ori	7.2×3.3	–
CW Leo	13.9×13.4	9.2×10.8
MWC 349	6.7×4.5	–
CRL 2688	$9.5 \times 2.1^{(2)}$	< 5
NGC 7027	8.8×7.6	$\simeq 10$
CepA	27.2 15.4	–

$^{(1)}$ Uncertain size, since map has poor quality.
$^{(2)}$ Mapped with the 19-channel bolometer of the MPIfR in December 1998.
Source sizes of less than about 10" are uncertain because the sources are basically unresolved and the derived sizes depends strongly on the adopted beam size (here: $\Theta_b = 10.8''$).

does not depend critically on how the source is orientated with respect to the beam, especially if there are slight pointing offsets or if the wobbler throw is so short that the off-position picks up extended emission. All our objects fullfill this condition to a satisfactory extent.

In Table 3 the source sizes derived from the maps are given, together with the sizes obtained at 800 μm with UKT14 at the JCMT (Sandell 1994). Most of the JCMT sizes were obtained by fully sampled maps, expect for the sources for which only upper limits are given, which were simply found to be point-like with respect to the beam of 19" in aperture photometry or five-point maps. The sizes at 1.2mm were obtained by fitting a two-dimensional gaussian to the map and deconvolving the obtained FWHM according to eq.(1).

The sizes found at 1.2 mm and at 800 μm are slightly different for many sources, the source sizes usually being larger at 1.2 mm. This might be due to the fact that the different wavelengths trace dust of different temperature or even, at long wavelengths, free-free emission. For GL 490 the large difference is most likely due to poor data quality of our maps and further observations of this object are necessary. For W3(OH) and K3-50A earlier maps exist done with the 7-channel bolometer at the 30m telescope (Reuter & Kramer 1998). They derived source sizes of 14 x 8" for W3(OH) and 10 x 11" for K3-50A. For K3-50A this agrees very well with our result while for W3(OH) we find a slightly larger source size. Since we have mapped W3(OH) several times and found roughly the same source size in each map, we are confident that our value is correct. Maybe a different effective frequency of the 7-channel bolometer and the present bolometer are responsible for the difference.

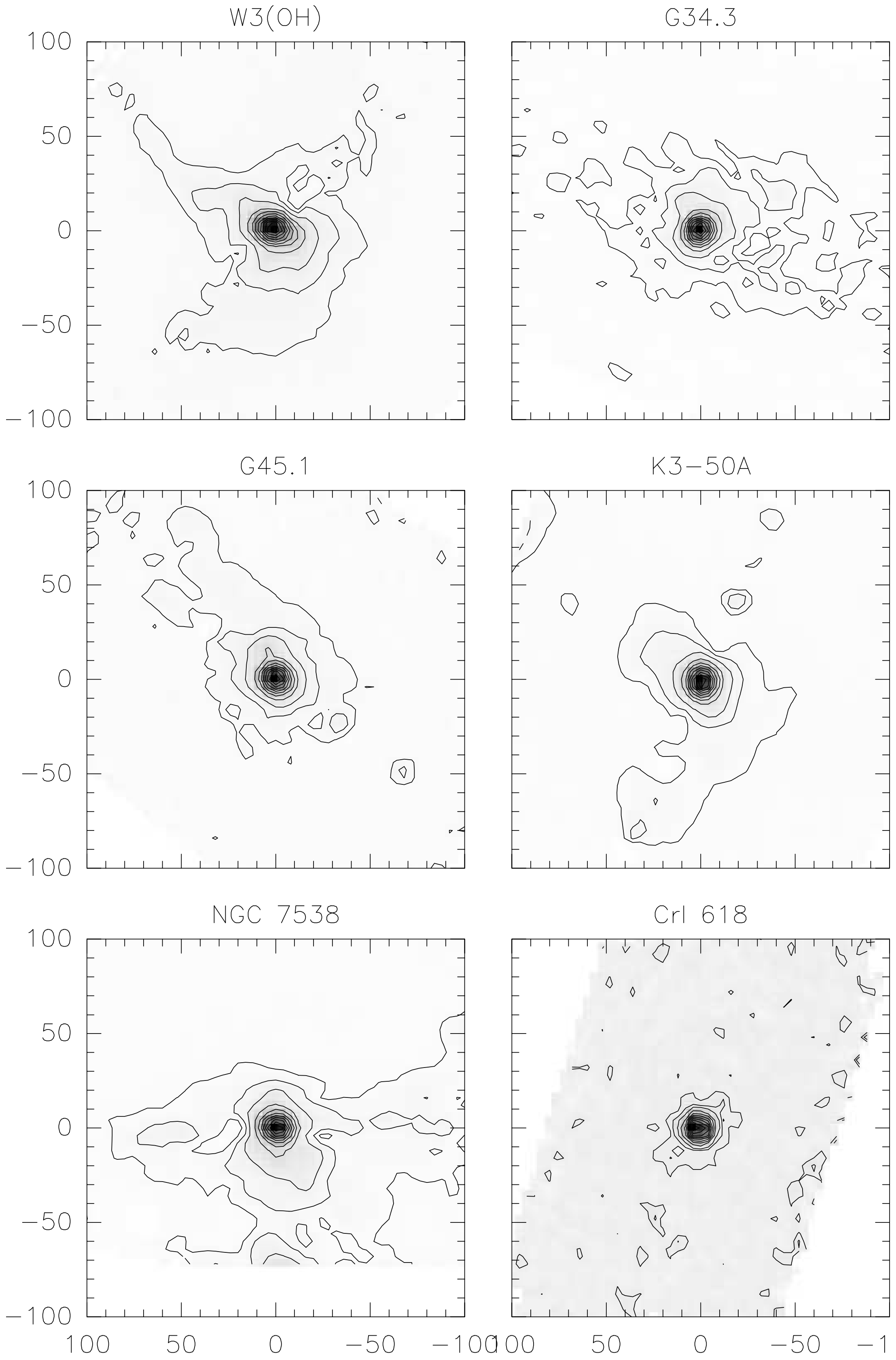

Figure 3: Maps of the sources. The contours are at 2, 5, 10, 20 .. 90% of the peak emission, expect of ALF Ori where the contours start at 10% of the peak emission and HL Tau and LKHα 234 where they start at 5%.

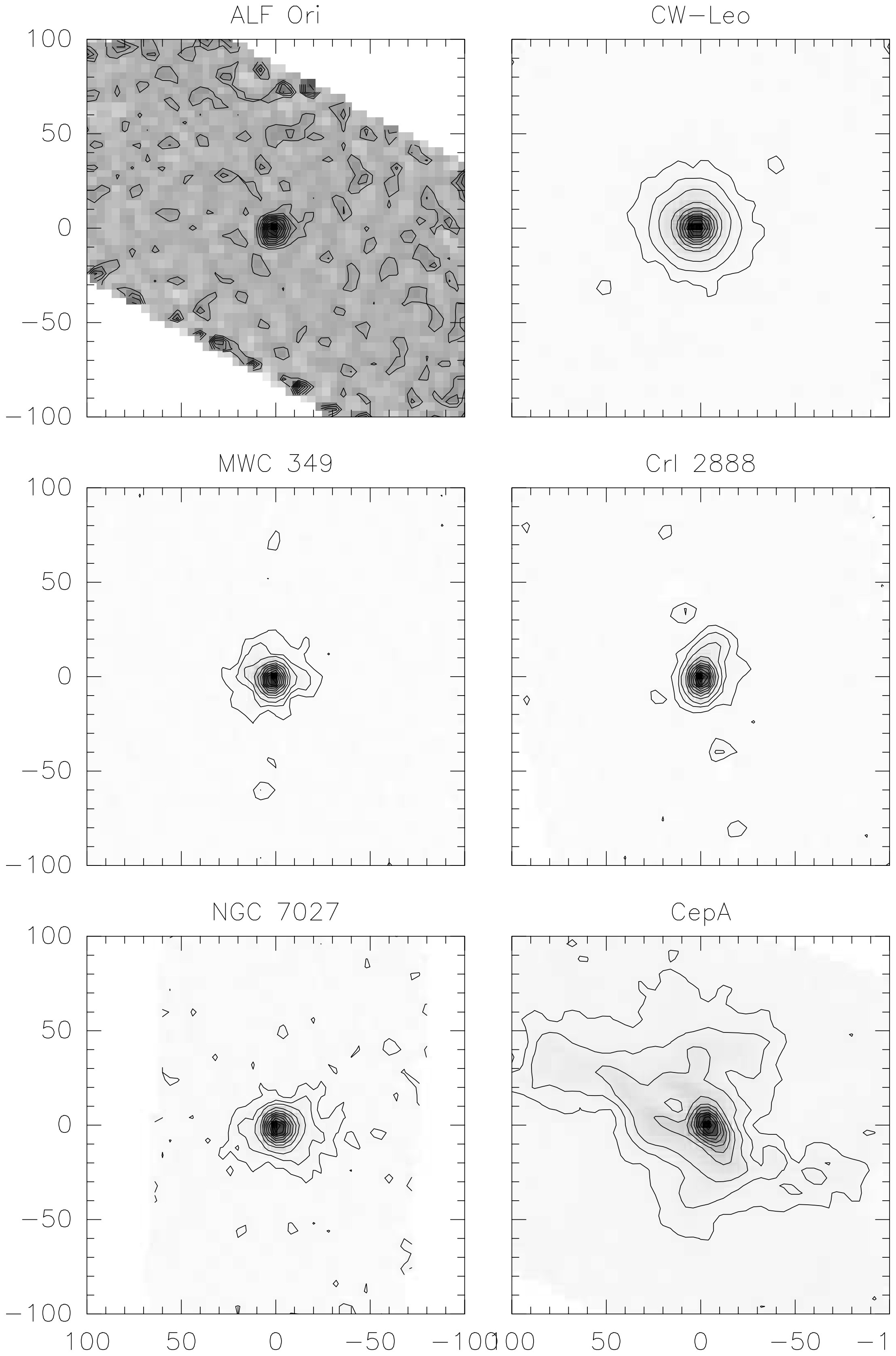

Fig.3 - continuing -

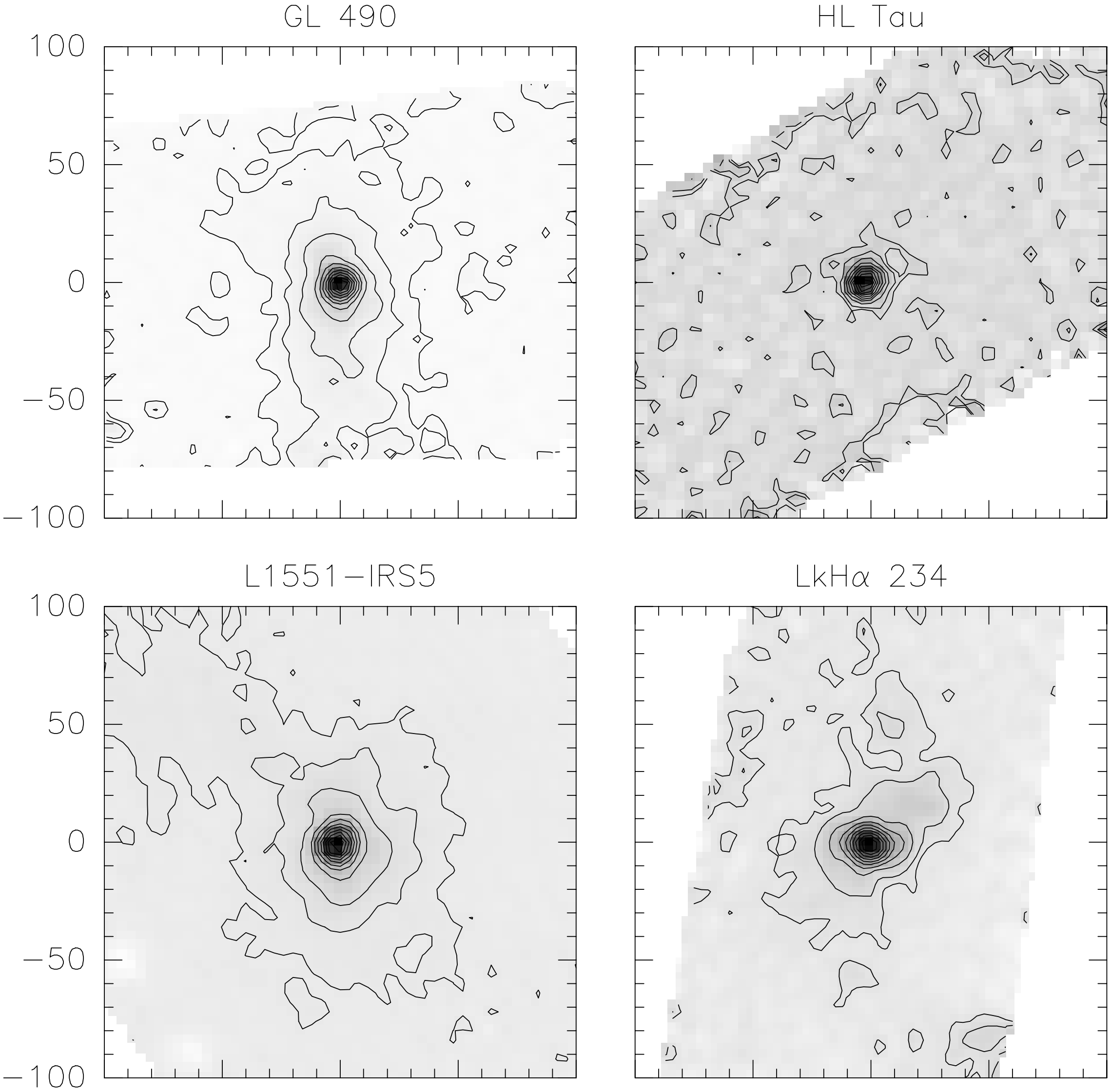

Fig.3 - continuing -

Table 4: Comparison of the flux densities at 228.9 GHz of the "standard" secondary calibrators measured with heterodyne receivers during the flux monitoring in 1995 – 1998, the extrapolated flux densities at 240 GHz and the flux densities measured with MAMBO

	$F_{228.9}$ [Jy/beam]	σ [Jy/beam]	n_{obs}	F^*_{240} [Jy/beam]	F_{bolo} [Jy/beam]
W3(OH)	6.51	0.80	14	6.95	6.98 ± 0.44
NGC 7538	4.85	0.65	16	5.57	5.69 ± 0.48
K3-50A	6.28	0.69	18	7.19	6.41 ± 0.19
NGC 7027	3.66	0.53	8	3.67	2.77 ± 0.10

* Extrapolated according to Reuter (private communication).

6 Comparison to other data

6.1 Comparison to IRAM heterodyne observations

W3(OH), K3-50A, NGC 7538 and NGC 7027 have been used as secondary calibrators for the flux monitoring of quasars at the 30m telescope and have been measured extensively at 87.7, 142.3 and 228.9 GHz with the heterodyne receivers. These data were calibrated with respect to Mars and/or Uranus. The flux densities at 228.9 GHz measured during the last years are given in Table 4, as well as the estimated flux at 240 GHz, the effective frequency of the bolometer, which was extrapolated by taking into account the spectral shape of the emission of the objects (Reuter & Kramer 1998 and Reuter, private communication). The agreement with the bolometer measurements (average value of years 1999 and 2000) is excellent for W3(OH) and NGC 7538. The difference for K3-50A is somewhat larger (12%) but still within the error limits and might be due to the steep increase of the spectrum at frequencies above 200 GHz which increases the uncertainty of the extrapolation. For NGC 7027 the differences is even 30%. The reason for this poor agreement is particularly unclear because NGC 7027 has a very flat spectrum so that neither an error in the effective frequency of the bolometer nor the uncertainty in the extrapolation should affect the comparison seriously.

6.2 Comparison to JCMT bolometer data

Some of our objects are also in the list of secondary calibrators of the JCMT (Sandell 1994). For these, the fluxes obtained with MAMBO and those obtained with UKT14 at the JCMT can be compared. The 1.3mm filter of UKT14 has an effective frequency of 238 GHz (Duncan et al. 1990, Tab. 2) and is thus very close to the effective frequency of MAMBO. We have to take into account the different beamwidths of the instruments and therefore calculate the total flux densities of the sources according to:

$$S_{tot} = S_{obs}\sqrt{\frac{\Theta^2_{s,a}}{\Theta^2_b}+1}\sqrt{\frac{\Theta^2_{s,b}}{\Theta^2_b}+1} \qquad (6)$$

where S_{obs} is the observed flux density per beam, $\Theta_{s,a}, \Theta_{s,b}$ are the major and minor axes of the sources (taken from Table 3) and Θ_b the HPBW of the beam.

Table 5: Comparison of the total fluxes obtained with MAMBO and those obtained with UKT14 at the JCMT (Sandell 1994)

Name	S_{JCMT} [Jy]	S_{IRAM} [Jy]	S_{JCMT}/S_{IRAM}
GL490	3.88 ± 0.15	4.75 ± 0.48	0.82
L1551-IRS5	2.87 ± 0.15	3.54 ± 0.39	0.81
W3OH	16.89 ± 0.76	17.55 ± 1.11	0.96
G34.3	34.44 ± 0.77	38.49 ± 1.43	0.89
G45.1	4.66 ± 0.13	5.17 ± 0.39	0.90
K3-50A	11.38 ± 0.52	12.25 ± 0.36	0.93
NGC7538	13.95 ± 0.63	15.79 ± 1.3	0.88
CRL618	2.58 ± 0.11	3.27 ± 0.14	0.79
CW-LEO	3.21 ± 0.61	3.39 ± 0.13	0.95
CRL2688	2.62 ± 0.11	2.63 ± 0.09	1.00
NGC7027	4.48 ± 0.12	4.36 ± 0.16	1.03

The comparison of our results with those listed in Sandell (1994) is given in Table 5. The adopted beams are 10.8" for MAMBO and 19" for UKT14 (Sandell 1994) and for the source sizes we take the results from the IRAM measurements (Tab. 4). The JCMT flux density for the variable source CW-LEO is approximated as the average of the maximum and minimum flux given in Sandell (1994).

There is a very satisfactory agreement between the flux densities derived at the two telescopes. The values derived at IRAM are slightly higher than the JCMT flux densities but the difference is small. The average ratio of the JCMT-to-IRAM flux is 0.91 ± 0.08. A possible reason for this difference could be the uncertainty in the source size, especially for objects where no sufficiently good IRAM maps exist. If we take the source size measured with the JCMT, the agreement between both fluxes improves slightly, the average ratio now being 0.99 ± 0.13.

7 Conclusions and summary

We have presented bolometer measurement of potential secondary calibrators obtained during two years. The agreement between the two years is very good, the average difference being less than 10%. We present a list of measured flux densities (Table 2) that allows observers to use these object as calibrators.

The maps of the sources have shown that, even though not all sources are point-like with respect to the beam, the extended emission is weak compared to the peak flux and reasonably symmetric. Comparison of the flux densities and source sizes obtained by IRAM to the flux densities and source sizes measured at the JCMT give a good agreement.

References

[1] Altenhoff, W.J., Thum, C., Wendker, H.J., 1994, A&A, 281, 161

[2] Brougiére, D., Neri, R., Sievers, A., 1998, IRAM Report

[3] Cernicharo, J., 1985, "ATM: A program to compute theoretical atmospheric opacities for frequencies up to 1000 GHz", IRAM Report

[4] Dutrey, A., Guilloteau, S., Duvert, G., Prato, L, Simon, M., Schuster, K., Ménard, F., 1996, A&A, 309, 493

[5] Kramer, C., 1997, "Spectral line calibration at the IRAM 30m radio telescope", IRAM Report

[6] Müller, T.G., Lagerros, J.S.V., 1998, A&A 338, 340

[7] Reuter, H.-P., Kramer, C., 1998, A&A, 339, 183

[8] Sánchez Contreras, C., Alcolea, J., Bujarrabal, V., Neri, R., 1998, A&A 337, 233

[9] Sandell, G., 1994, MNRAS, 271, 75